Integrated, Multi-Scale Characterization of Imbibition and Wettability Phenomena Using Magnetic Resonance and Wide-Band Dielectric Measurements

Semi-Annual Progress Report
April 1, 2005 to October 1, 2005

By

Mukul Sharma
Steve Bryant
Carlos Torres-Verdin

Work performed under Contract DE-FC26-04NT15518

Prepared for the U.S. Department of Energy
Dan Ferguson, Project Manager
U.S. Department of Energy
National Energy Technology Laboratory
One West 3rd Street, Suite 1400
Tulsa, OK 74103
918-699-2047

Prepared by
The University of Texas
Center for Petroleum and Geosystems Engineering
Austin, Texas 78712

SUMMARY

We have developed and validated a new pore-scale approach for the simulation of DC electrical resistivity measurements. The approach explicitly incorporates specific two-phase fluid distributions that are consistent with capillary pressure, saturation history, and percolation principles. Moreover, the simulation methodology properly reproduces pore-level fluid wettability, complex rock structure, and presence of conductive clay. We make use of a dynamic random-walk diffusion technique to simulate DC resistivity measurements via statistical averages of long-time diffusivity asymptotes. This strategy readily lends itself to accurately simulate the effects of explicit geometrical distributions of wetting films, pendular rings and snap-offs on DC resistivity measurements.

We reproduce sequential drainage/imbibition cycles and their corresponding resistivity-index cycles for both water-wet and oil-wet generic clean rocks. To our knowledge, this has not been achieved by any previously published pore-scale simulation method. The simulation methodology introduced in this repot can therefore be used as a tool to assess the influence of wettability and saturation history for specific conditions of grain size distributions. Classical values of *n* within specific ranges (less than 2, about 2, about 3, and larger) are all justified making use of wettability arguments. Non-constant values of *n* through the complete saturation range can therefore be explained and even predicted for simple rocks when given their saturation history; conversely, their saturation history can be inferred from simulations of resistivity index performed with similar models.

INTRODUCTION

Decrypting Archie's laws – Two of the most used electrical measurements in petrophysical analysis are the resistivity formation factor, $F_R = \rho_{Sw=100\%} / \rho_{bulk}$ (ratio of resistivity measured on a fully brine-saturated rock over the bulk resistivity of the brine), and the resistivity index, $I_R = \rho_{Sw<100\%} / \rho_{Sw=100\%}$ (ratio of the resistivity measured on a partially-saturated rock over that measured on a fully-water-saturated rock). Since Archie remarked that both resistivity indices correlated well with rock porosity ϕ (for F_R) and brine saturation S_w (for I_R) on a log-log plot for a collection of water-wet rock samples acquired from unrelated wells, it has been customary to relate these quantities via what became his two 'laws,' $F_R = a\phi^{-m}$ and $I_R = S_w^{-n}$. In these empiric power laws, the so-called "cementation exponent" *m* and "tortuosity factor" *a* are intended to capture the effect of rock tortuosity on the electrical current pathways through the pore space, while the "saturation exponent" *n* incorporates the additional electrical resistance created by the presence of electrically insulating hydrocarbons. Similar power laws were also derived for shaly sandstones based on empirical observations, with exponents corrected for the presence of clay double-layer conduction, as summarized by Bassiouni (1994) or Argaud *et al*. (1989). A profusion of experimental data has since shown that all these power-laws are far from being accurate as soon as the petrophysical conditions depart from the generic case of clean water-wet rocks with regular grain morphology. Extensive studies have been made of the physical origins of the variations of *m* with rock facies and will not be discussed here. More critical, in our view,

is the behavior of n, which in many cases depends on rock type, mineralogy, wettability, possibly porosity, and even S_w itself – which makes the power-law in a general sense not self-consistent

A need for uniformity – Since the 1950s, abundant literature documents experimental deviations from Archie's laws, and only in the last two decades have quantitative pore-scale models been available to understand some of the reported deviations in relation with percolation principles. In particular, pore networks have been widely used to assess the impact of pore connectivity and, above all, of fluid distribution, on capillary pressure and relative permeability with accuracy (e.g., Jackson *et al*., 2003; Gladkikh and Bryant, 2003). Simulation of resistivity hysteresis cycles, however, have not been as successful because many geometrical features of importance cannot be incorporated conveniently into these models – including conduction through thin films in water-wet rocks, pendular rings in oil-wet rocks, or just any presence of significantly conductive clay in general. Also, approximations made in pore networks remain strictly valid in distributions of relatively homogeneous pore and grain sizes, and therefore elude the analysis of complex rock morphologies including carbonate microporous, fractured or vugular rocks. For such complex rocks topologies, one usually relies on high-resolution digital cores (CT-scanned or statistically reconstructed). Voxel discretization of the medium, however, allows no accurate treatment of the fine rock microstructure (Liang et al., 2000), and no wettability effects can be directly assessed from such models – they are just used as skeletons to build new network models (Øren and Bakke, 2003) therefore again bound to the same limitations.

New approach – Our new approach allows the explicit and simultaneous incorporation at the pore scale of ***both*** rock morphology and wettability attributes within reasonable assumptions. Given the scale contrasts between the relevant geometrical features (nm-thick film, sub-μm micropores, μm-scale pores, sub-mm grains, mm-scale vugs), no numerical method seems more appropriate than unmeshed random walk trajectories with a variable step size. In the past, random walks have been applied successfully to simulate single-phase petrophysical measurements based on diffusion phenomena (DC conductivity and NMR) to disordered grain-packs or fractal rocks (Schwartz and Banavar, 1989), more recently to microporous carbonate rock models (Ramakrishnan *et al*., 1999; Toumelin *et al*., 2003), but never before consistently used with multi-phase fluid configurations. Our earlier attempts in the frame of NMR characterization (Toumelin *et al.*, 2004) neglected the percolation and snap-off effects inherent to realistic petrophysical models. In this new approach, we implement not only the pore geometries described by Kovscek *et al.* (1993) — now considered as the standard model for mixed-oil-wettability — but we also link it to a percolation model that remains consistent with saturation history and drainage/imbibition cycles based on simple heuristics. To summarize, our new model can explicitly incorporate:

- irreducible wetting-phase geometries, including thin films and pendular rings,
- percolation principles under the form of pore-to-pore propagation of non-wetting phase blobs (during wetting-phase drainage cycles) and snap-offs induced by the thickening of wetting layers (during wetting-phase imbibition cycles),
- distributions of clay-induced conductive double-layers in the form of spatial regions of electrical conductivity higher than that of pore water, and
- inhomogeneous rock and pore morphology, including intragranular and vugular porosity.

The objective of this report is to illustrate this new "perco-random-walk" approach with immediate results obtained for the case of a rock model that sets the standards in pore-scale modeling: the so-called "Finney pack" (Finney, 1970; Gladkikh and Bryant, 2003). After introducing the concepts and assumptions of the model in its generality, this report concentrates on applications concerning resistivity wettability effects with no clay or morphological effects, which will be left for future publications. We show that our model is general enough to reproduce a large spectrum of observed water-wet and mixed-oil-wet electrical phenomena despite the relative simplicity of the example pack.

UNIFORM PORE-SCALE FRAMEWORK FOR DC ELECTRICAL CONDUCTION, TWO-PHASE FLUID PERCOLATION, AND ELECTRICALLY CONDUCTIVE CLAY INCLUSIONS

Random-walk resolution for DC conductivity – Mathematically, both *resistivity* indices F_R and I_R can be expressed in terms of the *diffusion* tortuosity τ of the water phase in the pore space as (Bassiouni, 1994; Clennell, 1997; Rasmus, 1986; see also the Appendix):

$$F_R = \frac{\tau^2_{Sw=100\%}}{\phi} \overset{?}{\approx} \frac{1}{\phi^m} \tag{1}$$

and

$$I_R = \frac{1}{S_w}\left(\frac{\tau_{Sw<100\%}}{\tau_{Sw=100\%}}\right)^2 \overset{?}{\approx} \frac{1}{S_w{}^n}\,, \tag{2}$$

respectively.

Archie's laws attempt to capture macroscopic behavior which is mathematically linked to *electrical tortuosity* $\tau_e = L'/L$, the ratio between the distance, *L'*, measured along the path of electrical conduction between two points, and the straight-line distance, *L*, between the same two points. Although these conceptual definitions are regarded as of little practical interest because rock tortuosity cannot be measured in a direct manner, we make use of explicit pore-scale geometries specifically to *recreate* these tortuous conductive pathways in simplified rock models. As a result, it is possible to generate random-walkers which will diffuse in the water-filled zones of the geometrical model, and provide explicit quantitative indication of tortuosity from their long-time effective diffusivities. Once randomly created in the water-filled pore space, a random walker will iteratively jump by a distance δr dynamically determined by its location in the pore space under the criterion that δr be several times smaller than the smallest surrounding opening – e.g., the throat size of an occupied pore or the film thickness within a wetting water film. The duration δt of that displacement is given by Einstein's relation,

$$\delta r^2 = 6D_{wbulk}\ \delta t\,, \tag{3}$$

where D_{wbulk} is the bulk diffusivity of water. If the displacement takes the walker outside the water region, the walk time still increases by δt but the displacement is cancelled. At any given time, the normalized *effective* diffusivity is the ratio between the mean-square displacement over all diffusing walkers, and time, i.e.

$$\frac{D_w(t)}{D_{wbulk}} = \frac{\left\langle \left(r(t) - r(0) \right)^2 \right\rangle}{6t} . \tag{4}$$

As explained in the Appendix, the resistivity formation factor and resistivity index can be calculated from the long-time asymptotic of $D_w(t)$ as follows:

$$F_R = \frac{1}{\phi} \left(\frac{D_w(t \to \infty)}{D_{wbulk}} \right)_{S_w = 100\%} \tag{5}$$

$$I_R = \frac{1}{S_w} \left(\frac{\tau'^2}{\tau^2} \right) = \frac{1}{S_w} \frac{\left(D_w(t \to \infty) \right)_{S_w = 100\%}}{\left(D_w(t \to \infty) \right)_{S_w < 100\%}} . \tag{6}$$

To optimize the number of random walkers necessary to determine $D_w(t \to \infty)$ for a given pore configuration (saturation and imbibition/drainage cycle), and therefore the total running time, simulations where performed sequentially by series of 20 walkers. The resulting long-time effective diffusivities were averaged for as many series as needed (3 to 8), and for as long a simulated time necessary (10^5 to 10^7 ms equivalent diffusion time, for D_{wbulk} = 2 μm^2/ms) to reach unique asymptotic convergence within $\pm 5\%$ error bar or less.

Rock model – Figure 1 shows the grain pack used for the simulation results presented in this report. It consists of a 1600-μm size cubic arrangement of 100-μm grains whose coordinates were extracted from Finney's dimensionless dataset (Finney, 1970). Contrary to pore network models whose applications are restricted to rather uniform grain-size distributions, random-walk techniques allows the enforcement of any kind of grain pack and grain-size distribution (Schwartz and Banavar, 1989) – such as those used in Toumelin et al. (2004). These grain packs will be used in future work to study the impact of rock morphology on resistivity measurements, in combination with the effects solely due to wetting conditions considered in this report.

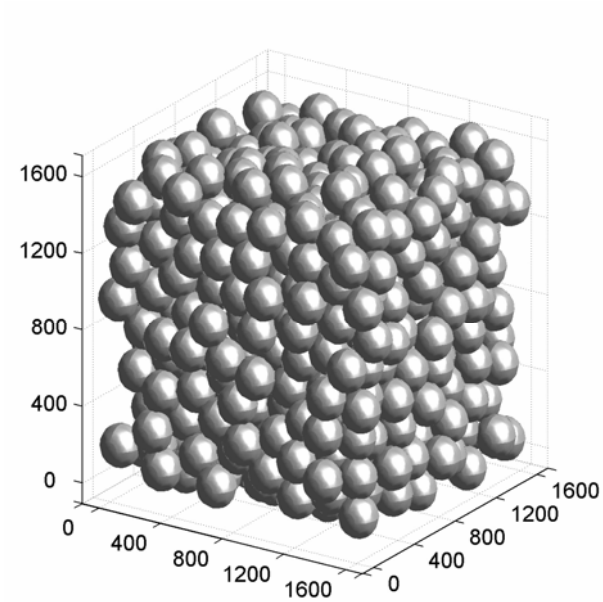

Fig. 1 *Example of sphere pack serving as rock skeleton for the random walkers (Finney pack with unique grain size). All dimensions are given in μm.*

Delaunay tessellation was then performed on the grain centers of the pack to divide the simulation volume into tetrahedral units joining all sets of the four-closest grains. In this example, the pack comprised 1000 spherical grains uniformly overgrown to reach 20% porosity units (p.u.), and involved 5857 Delaunay tetrahedra. A first random-walk simulation performed with only one fluid phase in the pore space determined the formation factor of this grain pack to be 12, which matches the one calculated by alternative pore-scale methods (Bryant and Pallatt, 1996). This figure is smaller than measured on 20 p.u. rocks, whose formation factors approach values between 18 and 20. However, as shown later in this report, such a difference does not prevent one from reproducing the main wettability effects on the resistivity index.

As illustrated in Fig. 2, each Delaunay cell defines one pore, four throats, and six pendular rings. The pore space is defined as the volume of the tetrahedron left after removal of the four apex grains, whereas the pore size properly speaking is here defined as the radius of the largest sphere that can be placed between these four grains, and the pore center is the center of that sphere. Similarly, on each triangular face of the tetrahedron we define a throat whose radius (and center) is equal to the radius (and center) of the largest circle that can be positioned in that plane between the three adjoining grains. The pendular rings are located in the water zone closer to the grain contacts (see more details below).

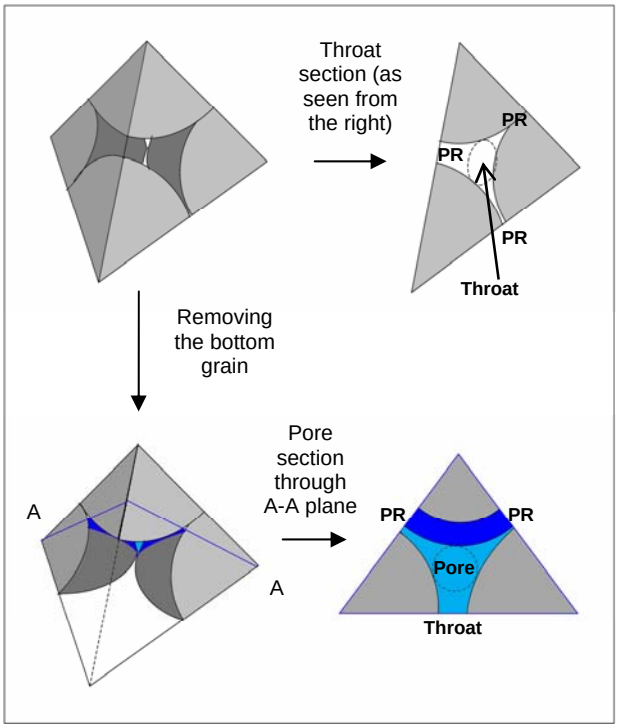

Fig. 2: *Graphical description of Delaunay tessellation used in this report to describe pore space and spatial distributions of fluids within the pore space. Each Delaunay tetrahedron relates a set of four closest grains. It defines one pore, four throats, and six pendular rings (PR).*

Two-phase fluid pore configuration – In order to efficiently parameterize the random walk, we define not only the grains (solid phase) but also the non-wetting fluid (water or hydrocarbon oil/gas phase, respectively) as a distribution of spheres which can ensure phase continuity throughout the simulation volume. The remaining pore space forms the wetting phase (oil or water, respectively, or both in mixed-wet cases). We define the geometry of pore "saturation types" by adapting the description previously advanced by Kovscek *et al.* (1993):

(1) **Fully water-saturated pores** are never touched by hydrocarbons: same as those represented in Fig. 2.

(2) **Invaded with hydrocarbon but still water wet**: the non-wetting phase is formed by the intersection between the pore volume and the sphere concentric with the pore and whose radius is the pore radius R multiplied by a factor α_o. As graphically illustrated in Fig. 3, water films of thickness T_w maintain water wettability at the rock surface, and pendular rings are formed by the pore space left at the intersection of the grains outside the hydrocarbon blob. Continuity of the wetting water phase from one tetrahedron to another is ensured through the pendular rings and the throats, while that of the hydrocarbon is only ensured if the blob size allows the filling of the throat. If the oil blob radius decreases and loses contact with all throats, or if the wetting films grow enough to fill all the throats, then snap-off of the oil blob occurs.

(3) **Invaded with oil and wettability altered into mixed-oil-wet**: all the fluid within the radius of the oil blob of Fig. 3 becomes oil and the water film disappears. Oil never enters the pendular rings and is now spatially anchored by wetting films which will remain in place even for the case of water re-invasion. Continuity of the oil phase from one tetrahedron to another is ensured through the pore throats, while that of the water is ensured through the pendular rings.

(4) **Invaded with water and wettability altered into mixed-oil-wet**: wetting films are now formed by oil and are located just at the intersection of the grain surface with the original oil blob (with radius $\alpha_o R$ concentric with the pore), with thickness T_o. The pendular rings remain water wet and water saturated, and the oil blob volume becomes water saturated. This is the geometry described by Kovscek as the mixed-oil-wet configuration with **unstable oil/water films**. In the case of stable oil/water emulsion film, oil lenses bridge the water pendular rings between the oil films of neighboring grains, thereby possibly trapping the water occupying the blob space and isolating it from the pendular rings. The stable oil/water film case is not as likely to occur as the unstable one (Hirasaki, 2004), and we therefore exclude it from the present study.

In this report, most drainage simulations are performed with film thicknesses T_w or T_o = 30 nm, which is meant to represent a realistic 10-nm thin film (Hirasaki, 1991). In the presence of slight grain-surface roughness, the assumed thickness would *behave* in equivalent fashion to a 30 nm thickness on our assumed smooth grain surface.

Percolation/drainage cycles: distribution of pore types in the rock – Different pore types are distributed within the Delaunay tessellation following the desired drainage or imbibition cycle and according to the distribution at the onset of that cycle (saturation history). More details on the description and simulation of each cycle are given in subsequent sections of this report. In general, the process follows simple percolation heuristics adapted from conventional models (Kovscek et al., 1993; Knight, 1991).

First, **drainage** cycles assume that non-wetting phase percolates in the form of αR–radius blobs from pore to pore starting on a face of the cubic simulation domain provided that all three following criteria are met:

(1) the blob which initiates percolation must be large enough to reach the throat leading to the pore candidate for drainage;
(2) the throat between the two pores is open to flow, i.e., the throat size is larger than the wetting film thickness, T;
(3) that throat exceeds a given threshold; as a key dimension of the process, the throat threshold for that saturation can be related to capillary pressure.

Imbibition is driven by a different process of film thickening. Starting from the thickness of the wetting film after drainage, the former is incrementally increased to T and the blob size is correspondingly decreased by βT in all the pores where the non-wetting phase is connected. When conditions (1) or (2) above are not met, then snap-offs occur. Because of the relative pore

and throat homogeneity of the Finney pack, snap-offs usually occur in stepwise fashion and not continuously. Therefore, increments in film thickness were constrained to produce a minimal number of snap-off increase per increment – from a few units up to several hundreds. When snap-off occurs in a pore, the non-wetting phase becomes disconnected from the rest of the non-wetting phase and no more film growth is allowed to take place in that pore.

During oil-wet imbibition cycles, it is particularly important to isolate the water snap-offs since those water regions will not contribute to electrical conduction. They must be discarded from the averaging included in equation (4), otherwise their finite long-term mean-square displacement will bias the calculation of effective diffusivity toward lower values (Schwarz, 2005). The same remark applies to any wettability type and imbibition/drainage cycle where isolated water exists (water trapped in any oil-wet rock, or disconnected water in pores with cemented throats in low-porosity grain packs).

Finally, any percolation/drainage cycle starts from the pore-type distribution resulting from the previous cycle and depends on one new parameter adjusted to conform with the specified fluid saturations.

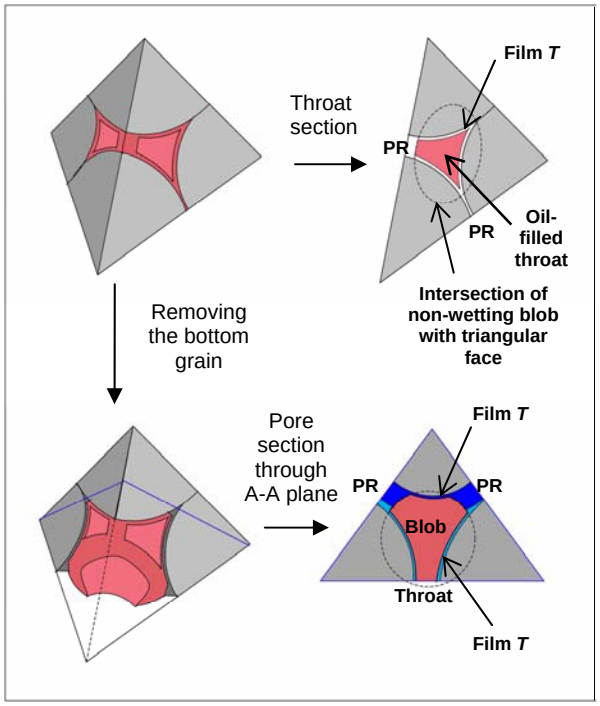

Fig. 3 *Graphical description of a two-phase saturation geometry in a Delaunay tetrahedron. A non-wetting blob occupies the intersection between the pore space and a sphere of radius R_o concentric with the pore shown in Fig.2. Thin wetting films of thickness T exist between the blob and the grains. In this case, R_o is large enough to reach the pore throat and allow percolation to a neighboring pore. A smaller R_o that would not allow reaching any pore throat of this*

tetrahedron (as well as thick wetting films completely filling all the pore throats) would snap-off the non-wetting blob.

Pore/clays dual pathways – As summarized by Argaud *et al*. (1989), all existing models (Waxman-Smits', Clavier's Dual-Water, Schwartz-Sen's, and Giouse-Argaud's DC models) for shaly sandstones can be mathematically described with the expression

$$I_R = S_w^{-n}\left(\frac{1+A}{1+A/S_w}\right) \tag{7}$$

on all or part of the saturation domain. In the above expression, the dimensionless parameter A captures the conductive efficiency of the clay double layers. Without going down to the molecular scale justifying cation exchange capacities, this parameter A was simply formulated from an effective viewpoint as the ratio between "excess conductivity associated with the clay conductor" and the bulk conductivity of the pore water. We make use of the approach to consider separate effective conductivities for the pore water, σ_{bulk}, and the clay-bound water, σ_{clay}, and to distribute the two values in different regions of the simulation volume. This strategy was implemented by Johnson *et al*. (1986) with random walks to model the effect of clay-coating conduction in single-phase, cubic-centered grain packs. Lima and Sharma (1989) also used this 'effective clay conductivity' model in an effective-medium-theory framework to account for both dispersed and coating clays (Almon, 1979), using published data on clay gels to parameterize σ_{clay}. In the present method, we combine both approaches and extend the random-walk application to disordered grain packs and two-phase fluid saturations to model spatial distributions of:

(a) dispersed clay pellets, considered as conductive grains from which the random walkers do not bounce, but where the walkers have a diffusivity equal to the pore water diffusivity multiplied by the conductivity contrast $\sigma_{bulk} / \sigma_{clay}$;
(b) pore-coating clays, treated as micron-thick layers surrounding the 'solid grain' spheres where random walkers change diffusivity; they do not bounce when crossing the clay/pore border, however they do bounce on the solid grain core from the clay coating.

As a guideline, clay conductivity is assumed "at least an order of magnitude more conductive than moderate salinity pore waters" (Almon, 1979). Consequently, the adopted model readily allows the integration of both spatial distributions of clays and wetting effects. Applications of this model are straightforward and will be the object of future developments and comparisons with shaly-sand electrical models. What follows specifically addresses the assessment of wettability effects and saturation on resistivity indices.

WATER-WET CYCLES

Cycle 1: drainage and reversible blob percolation – The originally fully water-saturated formation is first invaded with non-wetting hydrocarbons. The non-wetting phase is put in contact with one face of the cubic grain pack. Starting form each such inlet pore, the general drainage algorithm summarized previously is applied to allow pore-to-pore percolation of non-wetting oleic or gaseous phase, into successions of blobs of radii equal to $\alpha_o R$ (see remarks below concerning α_o). The wetting water layer of thickness T_w = 30 nm remains in contact with the entire grain surface, and compensates the grain surface roughness that our smooth-sphere model neglects. The water-wet rock drainage cycle yields the fluid configuration shown previously in Fig. 3.

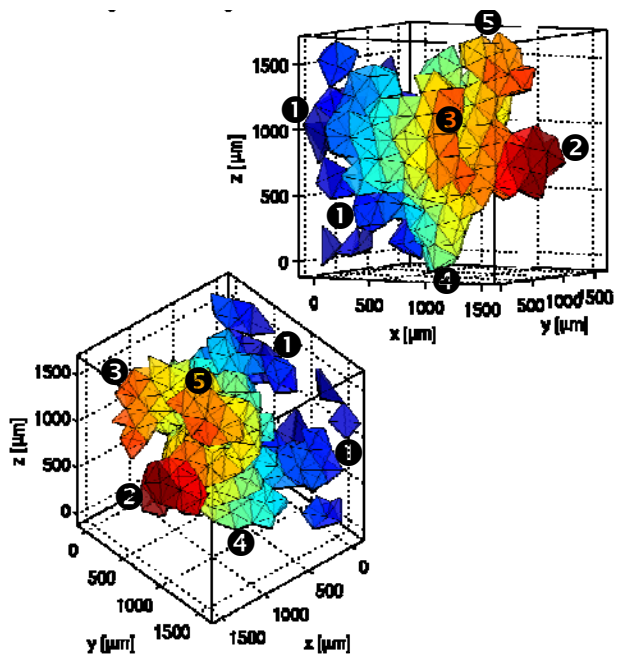

Fig. 4 *Visualization of Delaunay cells where oil percolated during Cycle 1 for an invasion of 22% oil saturation in the 20 p.u. Finney pack (17 µm throat threshold). The oil inlet is located at the face x=0 (circled 1's), and breakthrough is reached at the opposite face x=1600 µm (circled 2), as well as at faces y=0 (circled 3), z=0 (circled 4) and z=1600 µm (circled 5). The color scale describes the z-coordinate of the pore centers.*

As illustrated in Fig. 4, the above-described percolation algorithm provides a realistic representation of non-wetting phase percolation, where the non-wetting phase inlet is located on the left (x<0) and where percolation through the initially fully water-saturated pores reaches four of the five other sides of the cubic simulation domain. Note that no specific pressure gradient is imposed across the sample, and that the direction of drainage is just bound to the directional distribution of throat sizes; therefore, the imposed drainage is isotropic if the throat size distribution is also isotropic.

The blob radius factor α_o is adjusted for each grain pack to match the target irreducible water saturation when most pores are invaded with non-wetting phase (i.e., by setting a very small throat threshold). Irreducible saturation will be found in both the pendular rings and the pores which are the least connected. Since the throat size threshold controls the percolation process, it seems natural to relate the capillary pressure P_C (considered inversely proportional to the significant geometrical dimension at stake: radius of capillary tube, local curvature of pore walls, etc.) with the inverse of the throat threshold. Figure 5 shows such a *pseudo*-capillary-pressure curve for three values of α_o based on the 20 p.u. Finney pack. This curve exhibits the conventional features of capillary-pressure curves for primary drainage: (a) high curvature of P_C at high water saturation, (b) quasi-horizontal plateau and increasingly steeper P_C slope at decreasing water saturation, and (c) steep increase of P_C close to irreducible water saturation. This agreement is remarkable and corroborates the heuristics of the percolation algorithm.

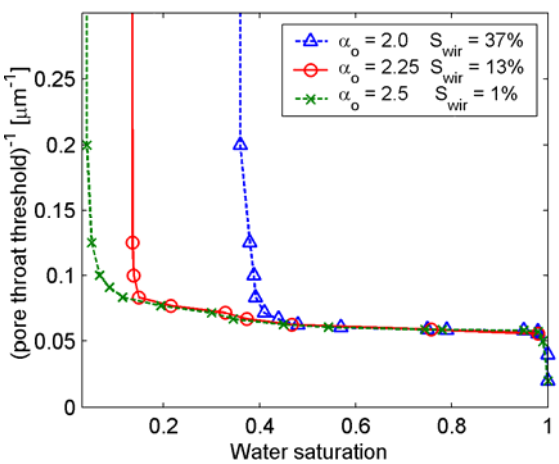

Fig. 5 *Pseudo-capillary-pressure curves for primary drainage in the 20 p.u. cemented Finney pack. The curves describe pseudo-capillary pressure values as a function of water saturation for different non-wetting blob size factors α_o involving different values of irreducible water saturation, S_{wir}.*

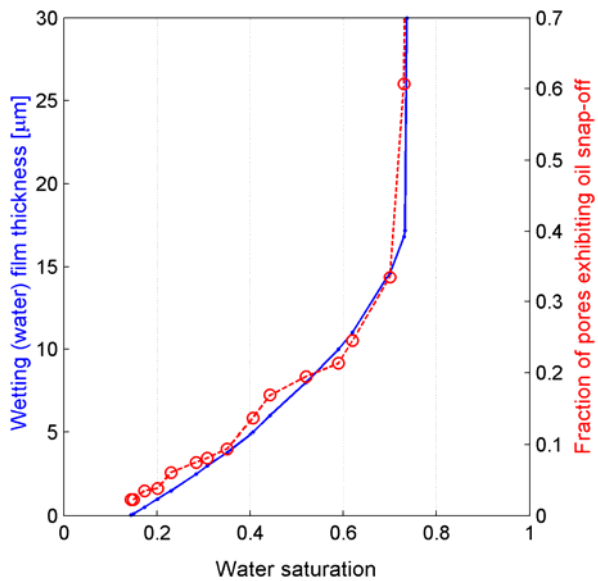

Fig. 6 *Evolution with (wetting) water saturation of: incremental water film thickness (left scale, plain curve with dot markers), and proportion of pores with oil snap-offs (right scale, dashed curve with circle markers).*

Cycle 2: primary imbibition and film-thickening/snap-off model – Two different processes are usually considered for imbibition: (a) the reverse process of the percolation-based drainage described above, involving no residual non-wetting saturation; or, (b) the process of wetting-film thickening yielding to snap-offs of non-wetting phase, as described earlier in general terms. The conditions necessary for one process or another to dominate the imbibition are not completely known; however, we modeled the film-thickening process to assess the theoretical effects of both processes.

Starting from the end of cycle 1 at 13% water saturation, iterative growth of the water film T_w and reduction of the non-wetting blob by $\beta_w T_w$ immediately creates oil snap-offs. The parameter that controls the maximal water saturation of the cycle (i.e., the saturation of snapped-off oil or gas) is this time the factor β_w. For the 20 p.u. Finney pack, values of β_w equal to 0.5 and 1 yielded irreducible oil/gas saturations of 27% and 13%, respectively. For this case we selected β_w = 0.5. Figure 6 shows the monotonically increasing film thickness and the corresponding number of snap-offs as functions of the water saturation for this cycle. Both curves overlap remarkably well as a signature of water wettability.

Resistivity-index hysteresis for Water-Wet cycles in generic 20 p.u. Finney pack – Cycles 1 and 2 were consecutively simulated based on the spatial fluid distributions discussed above. Figure 7 shows the resistivity indices, I_R, calculated along both cycles with respect to water saturation using a log-log convention so that n appears as the slope of the curve. The points simulated along the drainage curve match measurements made on a 20 p.u. clay-free sandstone sample (core T1 from Argaud *et al*., 1989) reasonably well, with a simulated value of n = 2.1. Random-walk results also compare well with pore network simulations obtained using the same Finney pack (Bryant and Pallatt, 1996), including a remarkable improvement around 50% water saturation. At

this saturation, the pore network simulations yielded a "jump" in resistivity index attributed to unaccounted electrical conduction through thin water films. Our simulations, which explicitly incorporate presence of water films also yields a slight increase of resistivity index at this value of water saturation, but exhibits a smoother and more realistic transition.

The second main feature of these water-wet simulations is the realization of a marked resistivity-index hysteresis when imbibition follows the film-thickening/snap-off process. During the latter cycle, the slope of I_R starts sharply at irreducible water saturation (high n value), then decreases and reaches the line $n = 1$ around 30% water saturation. At this saturation, only 7% of the pores have snapped-off, whereupon the incremental film thickness of 3 μm (3% of a grain radius) is present in most of the pores. Such a value of n is due to the fact that, for that film thickness, diffusion is hardly restricted, and therefore $I_R \simeq 1/S_w$.

This effect, in the absence of conductive clays, can explain I_R measurements where n is lower than 2. It is likely that a more realistic grain pack with a higher formation factor would include sufficient rock morphology effects to reduce this gap between values of n for imbibition and drainage. On the other hand, other published examples consistently exhibit no water-wet hysteresis between drainage and imbibition, which supports the notion of *reversible* blob percolation such as the one modeled in our drainage process.

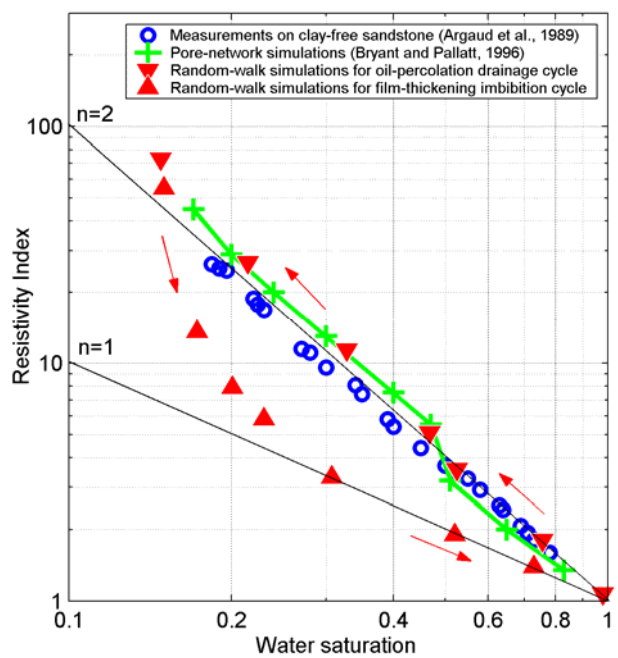

Fig. 7 *Evolution of resistivity index during primary drainage on a 20 p.u. clean water-rock rock: measurements performed on clay-free sandstones, pore-network simulation results with cemented Finney pack neglecting thin-film conduction, and random-walk simulation results carried out on the same ideal pack but allowing thin-film conduction. The imbibition cycle simulated for this pack also exhibits hysteresis*

Effect of surface roughness in shaly sands at high pore water conductivity – Diederix (1982) first reported measurements of clay-corrected resistivity indices of shaly sandstones that exhibited an abnormal decrease of *n* from 2.1-2.2 down to 1.3-1.5 below a critical water saturation close to 60%. The formation being salt-saturated, clay double-layer conduction was negligible compared to pore-water conduction, and therefore the rock electrically behaved as a clay-free saturated rock. No other petrophysical data are available from the wells considered in Diederix's (1982) study; however the reported clay-corrected values of *n* in the range of 2.1-2.2 support this assumption, since such values are usually observed for water-wet, clay-free sandstones (e.g., the water-wet data from Wei and Lile, 1991). The conductivity enhancement occurring below the critical water saturation was explained by Diederix (1982) as a consequence of the roughness created by the coating clay texture at the grain surface. He arrived at this conclusion by comparing the resistivity index of smooth and rough water-wet glass-bead samples.

We applied our model to reproduce the same phenomenon by arbitrarily increasing the wetting water film from 30 to 300 nm to account for clay surface roughness. Since clay conductivity was negligible, we did not make use of equivalent conductive clay regions. Figure 8 shows the corresponding simulation results along with the experimental trends taken from Diederix (1982). Surprisingly, both measured and simulated cut-off water saturations and "abnormal" 1.3-slopes agree well, especially given that no morphological effects, including porosity or formation factor, were ajusted in the simulations. This result proves that the negative curvature is indeed completely due to wetting effects, and that a wetting layer as thick as 0.3% grain radius was enough to reproduce it regardless of the assumed rock model.

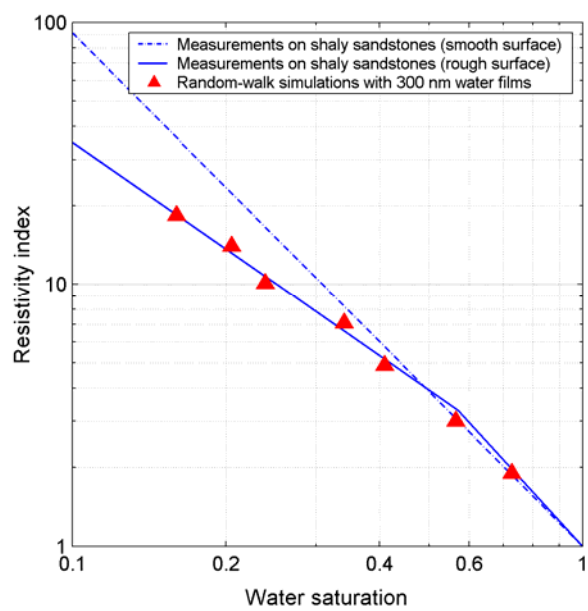

Fig. 8 *Influence of water film thickness on the resistivity index curve. Random-walk simulations with the 20 p.u. Finney pack and thick 300-nm water films agree well with measurements of clay-corrected resistivity index performed on shaly sandstones exhibiting negligible clay conductivity but surface roughness (Well 1 from Diederix, 1982). The remaining data points (Well 4 from*

Diederix, 1982), corresponding to similarly electrically negligible clay with smooth surface, agree well with the classical drainage behavior noted in Fig. 7.

MIXED-OIL-WET CYCLES

Cycle 3: wettability alteration – Over geologic time, depending on factors such as capillary pressure, grain curvature, or chemical composition of the fluids, an initially water-wet rock is likely to become at least partially oil-wet. Similar wettability alteration can also occur during oil-base mud-filtrate invasion at the near-wellbore scale. The Kovscek mixed-oil-wet model assumes a simplified cut-off between smaller pores which become oil-wet while larger pores remain water-wet. For the purpose of demonstration, we make the assumption that this partial wettability alteration is total and, as a result, all pores filled with oil up to irreducible water saturation have become mixed-oil-wet. Without loss of generality, we remark that only the case of unstable emulsion films is considered in this report. After complete wettability alteration, 3% of the fluids consist of isolated water that remains so for all oil-wet cycles.

Dual percolation system – From now on, the pendular rings are the only regions of the pore space that have remained water-wet. These pendular rings are spatially fixed by the wetting oil films, and their contribution to water invasion is very limited. Consequently, percolation was modeled as a dual phenomenon. On the one hand, the macroscopic fluid motion (drainage and imbibition) remains controlled by the pore throat openings, in a fashion similar to that of the water-wet case. On the other hand, electrical percolation through the rock is performed by both the water-filled pore throats (even though oil-wet), and the pendular rings. This condition makes it especially hard to model electrical percolation via pore network models. At each stage in the mixed-oil-wet drainage/imbibition cycle, connectivity of the water in a given pore must be checked through the neighboring tetrahedra which share the same throats (provided they are not plugged with oil) and the same pendular rings (provided the latter are themselves connected to a water-filled pore, otherwise they are isolated and hence do not allow electrical conduction).

Cycle 4: primary drainage – In a similar fashion to the water-wet scenario, oil films on the grain surface (except at pendular rings and pores filled with irreducible-water) have a thickness T_o set to 30 nm for all drainage simulations. The percolation algorithm exactly follows that of the water-wet case, with a parameter α_w equal to the previously set α_o, except in the presence of irreducible pores. Starting after cycle 3 at 13% irreducible saturation, 3 of which are trapped water, the evolution of saturation as a function of the throat threshold is tracked as a new pseudo-capillary-pressure curve, shown in Fig. 9, where the inverse throat threshold is plotted on a reverse axis to reflect the wettability change and maintain consistency with the water-wet case described in Fig. 5. This pseudo-capillary-pressure curve can be immediately compared to the theoretical oil-wet capillary-pressure curve calculated by Kovscek *et al.* (1993) and sketched in Fig. 10. If one postulates that a zero capillary pressure is obtained for a reciprocal pore threshold close to 0.65 μm^{-1}, one obtains a very good match between the two curves considering the rough assumption made on the inverse proportionality between capillary pressure and throat size.

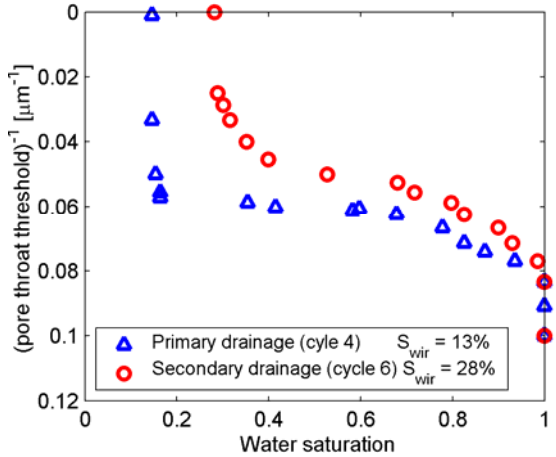

Fig. 9 *Pseudo-capillary-pressure curves simulated for primary and secondary oil-wet drainage cycles involving different values of irreducible water saturation, S_{wir}. The pore-throat threshold is plotted in reverse direction to reflect the oil wettability of the model. No irreducible oil is left in this model which assumes no oil-filled water-wet pore.*

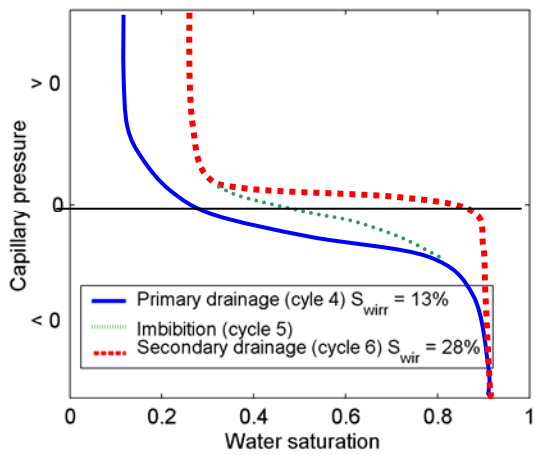

Fig. 10 *Theoretical capillary-pressure curves for oil-wet cycles that exhibit similar values of irreducible water saturation (adapted from Kovscek et al., 1993). Wettability is assumed only partially altered into mixed-oil-wet, thereby creating irreducible oil saturation.*

Cycle 5: imbibition – After enforcing a 90%-drainage (the absence of water-wet oil-filled water pore in this example prevents the build-up of irreducible oil saturation), imbibition with wetting oil is performed via the film-thickening model and a coefficient $\beta_0 = \beta_w = 0.5$. Figure 11 shows the evolution with wetting oil saturation of the incremental wetting oil film thickness and the amount of water trapped into snap-offs during imbibition. First, it is remarkable that the incremental oil wetting film thickness grows with wetting oil saturation in a manner identical to the incremental water-wetting film thickness with respect to the wetting water saturation described in Fig. 6. The build-up of water snap-offs and isolated water saturation, however, is very different from the water-wet case: instead of being progressive and proportional to the nominal film thickness, snap-offs occur suddenly above a threshold of 67% oil saturation, which

marks the irreducible water saturation for the snap-offs, the pendular rings, and the irreducible-water pores.

Cycle 6: secondary drainage – A new drainage cycle is sustained that progressively reconnects the water snap-offs as the throat drainage threshold decreases. Figure 9 shows the evolution of water saturation and pseudo-capillary pressure. This curve compares reasonably well with the theoretical curve shown in Fig. 10.

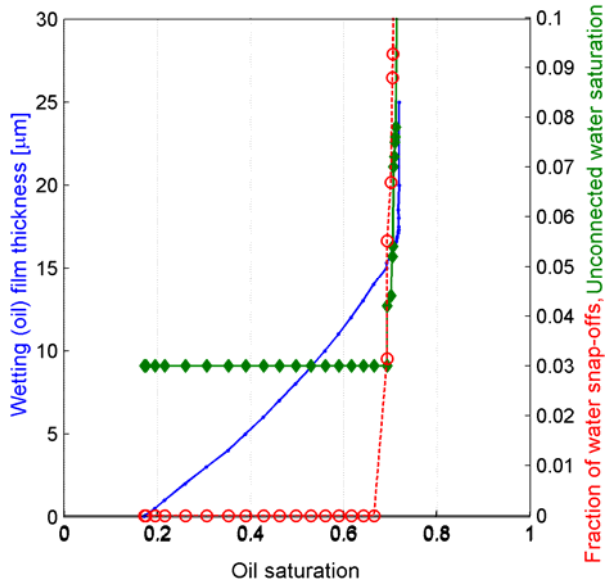

Fig. 11 *Evolution with (wetting) oil saturation of: incremental wetting oil film thickness (left scale, plain curve with dot markers), proportion of pores with water snap-offs (right scale, dashed curve with circle markers), and water saturation isolated from the water network (right scale, plain curve with diamond markers).*

Resistivity-index hysteresis for Mixed-Oil-Wet cycles – Results from random-walk simulations performed on the 20 p.u. Finney pack during mixed-oil-wet cycles 4 to 6 are plotted in Fig. 12. For comparison, Figure 13 shows the resistivity index measured on 19 p.u. oil-wet sandstone during similar cycles by Wei and Lile (1991). The qualitative agreement between the two figures is remarkable. The main differences are the irreducible saturation, for which the model may be tuned better, and the value of critical water saturation at which the saturation exponent increases abruptly during imbibition (about 40% with our model, 50% for the measurements). This critical saturation corresponds approximately to the saturation at which water snap-offs form abruptly. The sharp increase and decrease of resistivity index during cycles 5 and 6 is due to the fact that these isolated water blobs are not taken into account for the calculation of effective diffusivity or resistivity index (S_w in equation (6) only considers connected water saturation). However, the same water blobs do become part of the calculated total water saturation shown in the abscissa of Fig. 12.

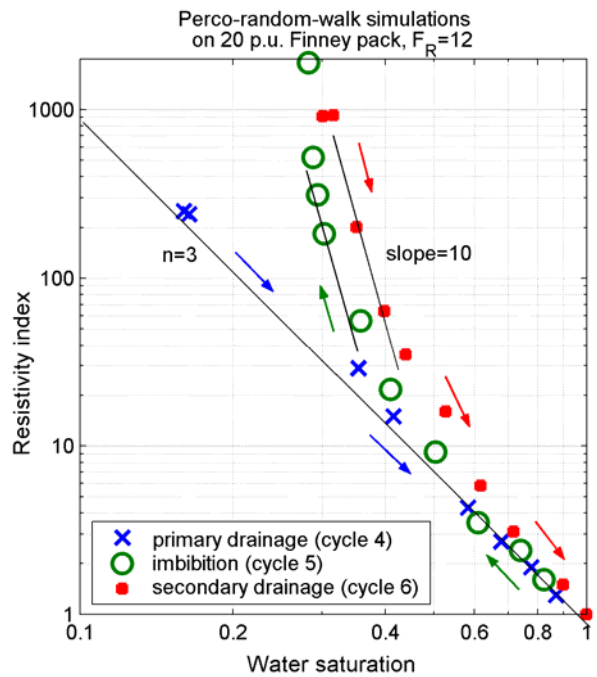

Fig. 12 *Resistivity-index hysteresis (cycles 4 to 6) simulated in a 20 p.u. Finney pack assuming mixed-oil-wet grains with no stable oil/water emulsion films. The lines n=3 and 10 are included for comparison with the measurements from Wei and Lile (Fig. 13)*

Previously, a few studies attempted to reproduce a similar "lower" hysteresis for the oil-wet resistivity index (formed by cycles 4 and 5). Sharma *et al*. (1991) could only reproduce the hysteresis cycle at high values of water saturation by incorporating wetting films. However, their formulation did not include a realistic rock/throat model. Man and Jing (2001), on the other hand, used more accurate throat geometries but did reached unrealistically low values of resistivity index in their oil-wet simulations, and no imbibition positive curvature. Zhou *et al*. (1997) did better to reproduce the "lower" hysteresis cycle based on a 3-dimensional cubic network based on the concept of effective percolation, but neglected specific rock morphology information. Remarkably, their oil-wet lower hysteresis exhibited the same critical saturation (40%) as the one we simulated with our model and the generic Finney pack. Such evidence supports the intuitive understanding that the incorporation of more realistic rock morphologies could reduce the difference between simulated and measured critical saturation.
Despite these efforts, to our knowledge the 'upper' hysteresis cycle formed by imbibition and secondary drainage (cycles 5 and 6) has never been reproduced numerically before this work.

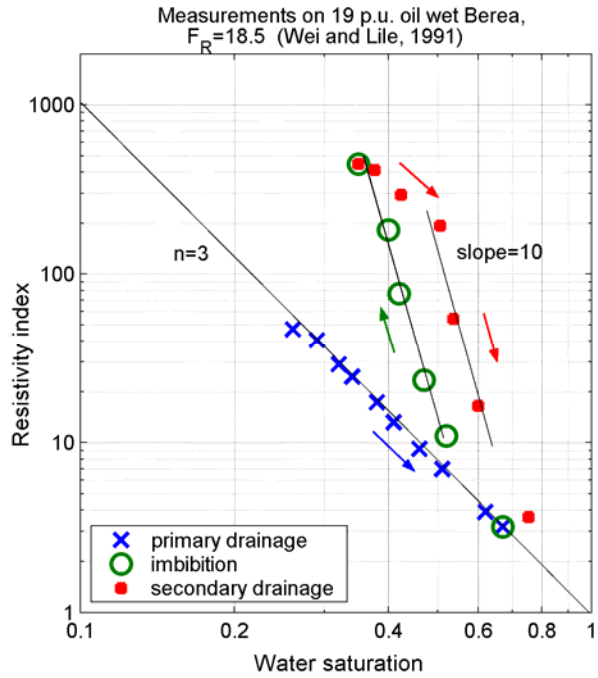

Fig. 13 *Resistivity-index hysteresis measured in 19 p.u. Berea plugs treated to remain oil-wet and saturated with 5-S/m brine and kerosene (Wei and Lile, 1991). Points marked with crosses, circles, and squares identify measurements simulated for our hysteresis cycles 4, 5, and 6, respectively.*

DISCUSSION

Our new model successfully reproduces a complete series of imbibition/drainage cycles for both water-wet and oil-wet rocks under the assumption of a relatively simple and homogeneous, although realistic, rock model. Several examples included in this report suggest the development of specific rock models with more realistic morphologies, not only to *fit* – which *not many* models can really do – but also to *predict* abnormal conductivity behavior in a general fashion – which *no* model properly does. As emphasized by Stalheim *et al*. (1999), rock morphology can have a strong impact on resistivity index/water saturation cross-plots. Intragranular porosity, in the form of microporosity or fractures, clay conduction pathways, certain vug types, or surface roughness, reduce the resistivity index of the saturated rock and create a negative curvature. Other kinds of vugs and oil-wettability increase the resistivity and create a positive curvature. Comparison of the oil-wet imbibition critical saturation measurements performed in sandstones by Wei and Lile (1991), (50%, also in Fig. 13), with those performed in carbonates by Sweeney and Jennings (1960) (40 and 80%) indicates that rock morphology cannot be discarded from a thorough analysis of DC electrical conduction phenomena in rocks. Fleury (2002) even reports completely non-linear resistivity index curves. By extension, a main challenge that remains far from solved is the accurate assessment of *n* when there are competing effects between wettability and morphology – for instance, for the case of a fractured carbonate (or as well a shaly sandstone) (negative-curvature effect) that is also oil wet (positive curvature).

Based on the approach proposed in this report, we were able to reproduce the effects of wettability on the DC electrical resistivity of saturated rocks – except for one important feature which deserves further analysis: Kovscek's stable oil/water emulsion lenses encountered in mixed-oil-wet drainage cycles. Additional work is also necessary to improve the accuracy of capillary pressure calculations during the water-wet and mixed-oil-wet imbibition and drainages cycles.

Compared to alternative pore-network models used to simulate the effective physical response of rock aggregates, the model-simulation framework advanced in this report embodies an accurate procedure to fill the gap between fluid, wettability, and rock structure. Such a diffusion-based framework will be particularly useful to also correctly reproduce and predict the influence of fluid type and wettability on NMR measurements performed on the same rocks as an extension of previous work (Toumelin *et al*., 2004).

SUMMARY AND CONCLUSIONS

We advanced and validated a novel pore-scale approach to simulate DC electrical conduction phenomena taking place in complex pore structures. This approach is based on percolation concepts, saturation history, and adaptive diffusion random walks; it was specifically used to assess wettability effects of rocks on DC resistivity measurements. To our knowledge, this is the first time that complete water-wet and oil-wet drainage, percolation, and hysteresis cycles and their influence on DC resistivity measurements were numerically simulated and successfully benchmarked against published reference measurements.

Classical values of n within specific ranges could be all theoretically justified making use of wettability arguments:

- Standard n values about 2 seem characteristic of water-wet rocks where the dominant fluid displacement process is blob-type percolation.
- In the absence of clay conduction, values of n smaller than 2 with positive hysteresis curvature are associated with water-wet rock imbibition close to irreducible water saturation. For the case of positive hysteresis curvature, such values are associated with water-wet rocks that exhibit substantial surface roughness, or microporous conductive paths.
- Notwithstanding probable additional rock morphology effects, values of n close to 1 can be theoretically expected for thick wetting films larger than 3% grain size.
- Through conductive layers doubling the wetting films, significant amounts of conductive clay will yield resistivity indices similar to observed for thick films ($n < 2$).
- Values of n about 3 are expected for homogeneous oil-wet clean rocks in their primary drainage at all saturations and for any subsequent imbibition/ drainage cycle for saturations higher than a critical value which depends on the rock morphology.
- Higher saturation exponents up to 10 can be expected in oil-wet rocks for saturations lower than that critical water saturation.

It was shown that water-wet hysteresis of resistivity index is theoretically possible with saturation regardless of rock morphology. On the contrary, the observed hysteresis of the oil-wet resistivity index can be explained by the sole effect of oil-wettability and water snap-off regardless of rock morphology.

The simulation methodology introduced in this can therefore be used as a tool to assess the influence of wettability and saturation history for specific conditions of grain size distributions. Slopes *n* of the resistivity index versus water saturation can vary across the saturation range and can be quantitatively explained – even predicted – for simple rocks when their saturation history is known. Likewise, saturation history can also be inferred from simulations of resistivity index performed with the models introduced in this report.

Finally, the pore-scale simulation approach described in this report is being currently extended to study the DC resistivity of shaly sands and inhomogeneous rock morphologies.

REFERENCES CITED

Almon, W.R., 1979: "A geologic appreciation of shaly sands," paper WW, SPWLA 20th Annual Logging Symposium.

Argaud, M., Giouse, H., Straley, C., Tomanic, J., and Winkler, K., 1989: "Salinity and saturation effects on shaly sandstone conductivity" (SPE paper 19577), SPE 64th Annual Technical Conference and Exhibition.

Bassiouni, Z., 1994: "Chapter 1 – electrical resistivity of rocks," in *Theory, measurement, and interpretation of well logs*, SPE textbook series vol. 4.

Bryant, S., and Pallatt, N., 1996: "Predicting formation factor and resistivity index in simple sandstones," Journal of Petroleum Science and Engineering **15**, 169-176.

Clennell, M.B., 1997: "Tortuosity: a guide through the maze," in Lovell, M.A, and Harvey, P.K. (eds.), *Developments in Petrophysics*, Geological Society Special Publication No. 122, 299-344.

Diederix, K.M., 1982: "Anomalous relationships between resistivity index and water saturations in the Rotliegend sandstone (The Netherlands)," paper X, SPWLA 23rd Annual Logging Symposium.

Finney, J.L., 1970: "Random Packings and the Structure of Simple Liquids. I. The Geometry of Random Close Packing," Proceedings of the Royal Society of London A **319**, November issue, 1539.

Fleury, M., 2002: "Resistivity in carbonates: new insights" (SPE paper 77719), SPE 77th Annual Technical Conference and Exhibition.

Gladkikh, M. and Bryant, S., 2003: "Prediction of interfacial areas during imbibition in simple porous media," Advances in Water Resources, **26** (6), June issue.

Hirasaki, G.J., 1991: "Wettability: fundamentals and surface forces," SPE paper 17367, SPE Formation Evaluation **6** (2), June issue, 217-226.

Hirasaki, G.J., 2004: personal communication.

Jackson, M.D., Valvatne, P.H., and Blunt, M.J., 2003: "Prediction of wettability variations and its impact on flow using pore- to reservoir-scale simulations," Journal of Petroleum Science and Engineering **39**, 231-246.

Johnson, D.L., Koplik, J., Schwartz, L.M., 1986: "New pore-size parameter characterizing transport in porous media," Physical Review Letters **57** (20), 2564-2567.

Knight, R., 1991: "Hysteresis in the electrical resistivity of partially saturated sandstones," Geophysics **56** (12), 2139-2147.

Kovscek, A.R., Wong, H., and Radke, C.J., 1993: "A pore-level scenario for the development of mixed wettability in oil reservoirs," AIChE Journal **39** (6), 1072-1085.

Liang, Z., Iaonnidis, M.A., and Chatzis, I., 2000: "Permeability and electrical conductivity or porous media form 3D stochastic replicas of the microstructure," Chemical Engineering Science **55**, 5247-5262.

Lima, O.A.L., and Sharma, M.M., 1990: "A grain conductivity approach to shaly sandstones," Geophysics **55** (10), 1347-1356.

Man, H.N, and Jing, X.D., 2001: "Network modelling of strong and intermediate wettability on electrical resistivity and capillary pressure," Advances in Water Resources **24**, 345-363.

Øren, P.E., Bakke, S., 2003: "Reconstruction of Berea sandstone and pore-scale modeling of wettability effects," Journal of Petroleum Science and Engineering **39**, 177-199.

Ramakrishnan, T.S., Schwartz, L.M., Fordham, E.J., Kenyon, W.E., Wilkinson, D.J., 1999: "Forward models for nuclear magnetic resonance in carbonate rocks," The Log Analyst **40** (4), 260-270.

Rasmus, J.C., 1986: "A summary of the effects of various pore geometries and their wettabilities on measured and in-situ values of cementation and saturation exponents," paper PP, SPWLA 27th Annual Logging Symposium.

Schwartz, L.M., Banavar, J.R., 1989: "Transport properties of disordered continuum systems," Physical Review B **39** (16), 11965-11970.

Schwartz, L.M., 2005: personal communication.

Sharma, M.M., Garrouch, A., and Dunlap, H.F., 1991: "Effects of wettability, pore geometry, and stress on electrical conduction in fluid-saturated rocks," The Log Analyst, September-October issue, 511-526.

Stalheim, S.O., Eidesmo, T., and Rueslåtten, H., 1999: "Influence of wettability on water saturation modelling," Journal of Petroleum Science and Engineering **24**, 243-253.

Sweeney, S.A., and Jennings, H.Y.: "Effect of wettability on the electrical resistivity of carbonate rock from a petroleum reservoir," J. Phys. Chem. **64**, May 1960.

Toumelin, E., Torres-Verdín, C., Chen, S., and Fischer, D.M., 2003: "Reconciling NMR measurements and numerical simulations: assessment of temperature and diffusive coupling effects on two-phase carbonate samples," *Petrophysics* **44** (2), March-April issue, 91-107.

Toumelin, E., Torres-Verdín, C., Sun, B., and Dunn, K.-J., 2004: "A numerical assessment of modern borehole NMR interpretation techniques" (SPE paper 90539), SPE 78th Annual Technical Conference and Exhibition.

Wei, J.-Z., and Lile, O.B., 1991: "Influence of wettability on two- and four-electrode resistivity measurements on Berea sandstone plugs" (SPE paper 21628), SPE Formation Evaluation **6** (4), December issue, 470-476.

Zhou, D., Arbabi, S., and Stenby, H.: "A percolation study of wettability effects on the electrical properties of reservoir rocks," Transport in porous media **29**, 85-98.

APPENDIX

Diffusion tortuosity and conduction tortuosity: why a random-walk simulation of DC conductivity phenomena? – The parallel between diffusion and conduction transport processes lies in their common Laplace equation at steady state. For diffusion, D is the diffusivity and C the concentration of a soluble species and

$$\nabla \cdot \left(D \nabla C \right) = 0 .$$

At steady state, D and C are macroscopically constant and do not vary with time (t). The associated diffusion tortuosity (with the same definition as above, but considering molecules instead of current) is calculated as:

$$\tau^2 = \left(\frac{D(t \to \infty)}{D_{bulk}} \right)^{-1} > 1 .$$

This ratio, on the other hand, is the long-time limit of the ratio of the mean-square displacement of the soluble species over the diffusion time, i.e.,

$$\frac{D(t)}{D_{bulk}} = \frac{\left\langle \left(r(t) - r(0) \right)^2 \right\rangle}{6t} .$$

For electrical transport phenomena, σ is the electrical conductivity of the medium and V is the electrical potential. By enforcing macroscopic equilibrium one obtains

$$\nabla \cdot \left(\sigma \nabla V \right) = 0 .$$

In a fashion similar to the analytical treatment of diffusion, the electrical tortuosity is given by

$$\tau_e^{\,2} = \left(\frac{\sigma(t \to \infty)}{\sigma_{bulk}} \right)^{-1} > 1 .$$

As detailed by Clennell (1997), a correction factor of $1/\phi$ is required to relate diffusion tortuosity and electrical tortuosity, whereupon

$$F_R = \frac{\rho(t \to \infty)}{\rho_{bulk}} = \left(\frac{\sigma(t \to \infty)}{\sigma_{bulk}} \right)^{-1} = \frac{\tau^2}{\phi} .$$

If one now considers the effective diffusivity of water, which is the conductive phase, in terms of diffusivities, F_R can be written as

$$F_R = \frac{1}{\phi} \left(\frac{D_w(t \to 0)}{D_w(t \to \infty)} \right)_{S_w = 100\%} .$$

Consequently, the latter expression can be calculated via diffusing random walkers reproducing the Brownian motion of water molecules.

Similarly, the resistivity index expressed as a function of tortuosities can be written as a function of the ratio of diffusivities, namely,

$$I_R = \frac{1}{S_w} \left(\frac{\tau'^2}{\tau^2} \right) = \frac{1}{S_w} \frac{\left(D_w(t \to \infty) \right)_{S_w = 100\%}}{\left(D_w(t \to \infty) \right)_{S_w < 100\%}} .$$

The above expression can also be calculated from the long-time asymptote of the effective diffusivities of the saturated rock model at different saturations.